HHS Public Access

Author manuscript

Mol Cancer Ther. Author manuscript.

Anti-tumor activity of a novel LAIR1 antagonist in combination with anti-PD-1 to treat collagen-rich solid tumors

B. Leticia Rodriguez[1], **Jiawei Huang**[2], **Laura Gibson**[1], **Jared J. Fradette**[1], **Hung-I H. Chen**[2], **Kikuye Koyano**[2], **Czrina Cortez**[2], **Betty Li**[2], **Carmence Ho**[2], **Amir M. Ashique**[2], **Vicky Y. Lin**[2], **Suzanne Crawley**[2], **Julie M. Roda**[2], **Peirong Chen**[2], **Bin Fan**[2], **Jeong Kim**[2], **James Sissons**[2], **Jonathan Sitrin**[2], **Daniel D. Kaplan**[2], **Don L. Gibbons**[1,*], **Lee B. Rivera**[2,*]

[1]Department of Thoracic/Head and Neck Medical Oncology, The University of Texas MD Anderson Cancer Center, Houston, TX, USA.

[2]NGM Biopharmaceuticals Inc. South San Francisco, CA, USA.

Abstract

We recently reported that resistance to PD-1-blockade in a refractory lung cancer-derived model involved increased collagen deposition and the collagen-binding inhibitory receptor leukocyte-associated immunoglobulin-like receptor 1 (LAIR1), and thus we hypothesized that LAIR1 and collagen cooperated to suppress therapeutic response. Here, we report LAIR1 is associated with tumor stroma and is highly expressed by intratumoral myeloid cells in both human tumors and mouse models of cancer. Stroma-associated myeloid cells exhibit a suppressive phenotype and correlate with LAIR1 expression in human cancer. NGM438, a novel humanized LAIR1 antagonist monoclonal antibody, elicits myeloid inflammation and allogeneic T cell responses by binding to LAIR1 and blocking collagen engagement. Further, a mouse-reactive NGM438 surrogate antibody sensitized refractory KP mouse lung tumors to anti-PD-1 therapy and resulted in increased intratumoral CD8+ T cell content and inflammatory gene expression. These data place LAIR1 at the intersection of stroma and suppressive myeloid cells and support the notion that blockade of the LAIR1/collagen axis can potentially address resistance to checkpoint inhibitor therapy in the clinic.

[*]**CORRESPONDING AUTHORS:** Dr. Don L. Gibbons, Department of Thoracic/Head and Neck Medical Oncology, The University of Texas MD Anderson Cancer Center, 1515 Holcombe Blvd, Unit 432, Houston, Texas, 77030. USA, dlgibbon@mdanderson.org, Dr. Lee B. Rivera, NGM Biopharmaceuticals Inc. 333 Oyster Point Blvd. South San Francisco, California, 94080. USA, lrivera@ngmbio.com.

Author contributions: B.L.R, L.B.R., and D.L.G. conceived and designed the studies. J.H, S.H., J.F., L.G., C.C., B.L., C.H., A.A., V.Y.L., J.M.R., K.C., H.H.C., B.F., J. K., J.S., J.S., L.B.R., B.L.R., and D.L.G developed assays, performed and interpreted the experiments. H.C, and K.K. performed bioinformatics and statistical analysis. L.B.R, D.D.K., and D.L.G. supervised the participants. B.L.R., L.B.R., and D.L.G. wrote/edited the manuscript.

Authors Disclosures: J.H, C.C., B.L., C.H., A.M.A., K.M., V.Y.L., J.M.R., K.C., H.H.C., Y.W., B.F., J. K., I.M., J.S., J.S., D.D.K., H.T. and L.B.R. are current or former employees of NGM Biopharmaceuticals. D.L.G. has served on scientific advisory committees for AstraZeneca, Sanofi, Menarini Ricerche, 4D Pharma, Onconova, and Eli Lilly, and has received research support from Janssen, Takeda, Ribon Therapeutics, Astellas, NGM Biopharmaceuticals, Boehringer Ingelheim and AstraZeneca. No potential conflicts of interest were disclosed by the other authors.

The authors declare no potential conflicts of interest.

INTRODUCTION

Immunotherapy has dramatically changed the treatment landscape for patients diagnosed with solid and liquid cancers. Despite advances in the field, a significant fraction of patients either fail to respond or develop acquired resistance during treatment with immune checkpoint blocking agents [1]. Thus, efforts to uncover the nature of such resistance are needed to develop more effective therapeutic strategies. Such efforts have identified the collagen-rich stroma as a potential source of resistance, warranting innovative approaches to target this compartment in the context of checkpoint inhibitor therapy [2,3]. Our group and others have shown that acquired resistance to immune checkpoint blockade is associated with collagen deposition in the tumor microenvironment [4]. Further, collagen prevalence correlates with poor prognosis in diverse cancers, suggesting the extracellular matrix (ECM) is also involved in disease progression [5–7]. While therapeutics that modulate ECM remodeling such as MMPs have been proposed, they are mostly ineffective due in part to lack of specificity and undesirable side effects [8].

As collagen has been demonstrated to regulate both T cell activity and macrophage function, stroma-derived resistance likely arises at the intersection of ECM and immune cell interactions [9–11]. Immune cells can express a variety of collagen receptors, including the receptor tyrosine kinase DDR1, adhesion-promoting integrins, and the ITIM-containing inhibitory receptor LAIR1 [12]. LAIR1 is a hematopoietic lineage-restricted collagen receptor reported to regulate diverse responses across both innate and adaptive immune cell types, including activation, differentiation, and antigen recognition [13]. Therefore LAIR1/collagen engagement represents an immune modulating function of the ECM and an opportunity for tumors to inhibit antitumor immune response [14–16].

Indeed several groups have proposed strategies to disrupt the collagen-LAIR1 interaction [4,17–19].

We propose that specific inhibition of LAIR1/collagen engagement will restore immune cell functionality and cytotoxicity, thus enabling response in otherwise resistant tumors. In the current study, we assessed the association of LAIR1 with stroma in human cancer and describe a novel LAIR1/collagen antagonist. We found that LAIR1 expression was higher in tumors with abundant stroma in most solid tumor indications, and that the majority of intratumoral LAIR1 content was derived from the myeloid compartment. Using spatial transcriptomic profiling, we found that stroma-associated myeloid cells are distinct from their non-stromal counterparts, having features of immunosuppressive cells and correlating with LAIR1 expression in cancer. NGM438, a novel monoclonal antibody antagonist of LAIR1/collagen engagement, potently polarized collagen-suppressed myeloid cells and activated collagen-suppressed T cells. Finally, we show that a mouse reactive NGM438 surrogate antibody combined with anti-PD-1 blocks primary and metastatic tumor growth in refractory, stromal-rich tumor models.

MATERIALS AND METHODS

Staining of human tumor sections

Tissue sections from HNSCC, PDAC, NSCLC, or RCC were cut at 4 μm and baked at 60°C for 2 hours. IHC was performed using a Bond Polymer Refine Detection kit on the Leica Bond Rx autostainer, which included dewaxing, heat-induced epitope retrieval, antibody incubation, signal detection, and hematoxylin counterstaining. LAIR1 was detected using anti-LAIR1 clone NKTA255 (ThermoFisher; MA1–33620). Slides were removed from the autostainer, rinsed in water, dried, and cover slipped using Surgipath MM 24 Mounting Media. Slides were scanned at the 40X magnification using a Leica Aperio AT2 slide scanner. Patient n; HNSCC = 30, NSCLC = 27, PDAC = 13, RCC = 31. Adjacent tumor sections were stained for collagen using Pico Sirius red.

TCGA analyses

Gene expression data were analyzed using Omicsoft Land B37 (Qiagen). Gene sets were assessed by compiling aggregate gene sums, and quartiles were defined within individual indications. LAIR1 gene expression and TME gene sums were exported and analyzed using Graphpad Prism software. Data from normal tissues were excluded from all analyses. Gene sets queried in the TCGA include the TGFβ dominant gene set used to assess ECM (*COL1A1*, *COL3A1*, *COL5A1*, *COL6A1*, *COL6A3*, *TIMP1*; [20]) and the gene set enriched in SAM (*TPSAB1, F13A1, CCL13, CD163, FOLR2, CCL2, TCRB, ADAM19, WIPF1, SEPP1, DUSP1, GEM, MRC1, OLFML2B, HSPA6, RCN3, FCGR2C, FGD2, TMEM176B, GIMAP7, RASSF4, TSC22D3, LRRC15, CCL18, LTB, DAB2, EMB, RUNX1, PLTP, CIITA, RASA3, CYTIP, PRDM1, HERPUD1, STAB1, MAF, SLC40A1, ANXA6, GADD45B, GGTA1P, PARVG, TRAF1, MCTP1, LCP2, HLA-DPB1, LYZ, LGALS1, GGT5, HLA-DQA1, SLCO2B1, HLA-DPA1, MAFB, LIX1L, TXNIP, CCL8, HLA-DRB1, RGS2, FPR1, PDK4, HLA-DRA, CXCR4, EMP3, ANKRD44, AMICA1, JAK3, TMEM176A, ZFP36, SORCS2, CD74, ARHGEF10L, CLMP, ARHGDIB, HLA-DQB1, HGF, FYN, LIMD2, CD69, CLEC7A, TNFAIP3, GLCCI1, TRAC, P2RY13, CDC42EP3, CYP1B1, S100A4, PTPRCAP, CD6, NEK6, SFTPD, DIO2, ARHGEF1, RENBP, ZEB2, PFKFB3, SORBS3, VSIG4, NBPF14, VIM, PRKCB, SLAMF8, RUNX2, ALOX5, RGL1, TBC1D10C, LILRA4, IL2RA, CXCL12, HSD11B1, LPXN, CD5, FCGR1A, PIWIL2, ISM1, GNMT, DOCK2, TGFBR2, MMP3, SERPING1, MARCKS, GPC6, APOD, LOX, CITED2, AIF1, NOTCH2NL, SLC1A3, SH3BGRL*, and *FKBP5*).

Analysis of single cell RNAseq datasets from human and mouse

All single cell RNAseq datasets and cell type annotations were previously described. For the NSCLC dataset [21], myeloid cells were defined by the myeloid cluster; T cells were defined by the T_cell cluster; and others were defined by combining B_cell, tumor, alveolar, endothelial cell, fibroblast, and epithelial cell clusters. For the breast cancer dataset [22], myeloid cells were defined by combining macrophage, monocyte:precursor, monocyte, neutrophil, mDC, and MAST clusters; T cells were defined by combining T:CD4+Naïve, T:CD8+EM, T:CD8+Naïve, T:CD4+CM, T:CD4+EM, T:Reg, and T:CD8+CM clusters; and others were defined by combing NK:CD56+16+3+NKT, B, NK:CD56+16+3-, pDC, and NK:CD56–16+3- clusters. For the PDAC dataset [23,24], myeloid cells were defined by the

macrophage cluster; T cells were defined by the T cell cluster; and others were defined by combining Ductal cell type 2, Stellate cell, Endothelial cell, Ductal cell type 1, Fibroblast cell, B cell, Endocrine cell, and Acinar cell clusters. For the CRC dataset [25], myeloid cells were defined by combining the myeloid and Mast clusters; T cells were defined as the T/NK/ILC cluster; and others were defined by combining Epithelial, B, Plasma, and Stromal clusters. For the RCC dataset [26], myeloid cells were defined by combining FOLR2-Hi TAM, GPNMB-Hi TAM, VSIR-Hi TAM, CD16+/− Monocyte, CXCL10-Hi TAM, DC, Cycling TAM, and Mast cell clusters; T cells were defined by combining Effector T-Helper, Cycling CD8+ T cell, CD8+ T cell, T-Reg, and Memory T-Helper clusters; and others were defined by combining FGFBP2+/− NK, NKT, and Cycling Tumor clusters. For the pan-can mouse dataset [27], myeloid cells were defined by the macrophage cluster; T cells were defined by the T cell cluster; and others were defined by combining CT26, MC38, LL2, EMT6, B16F10, SA1N, CAF, and pDC clusters. For the T3 mouse tumor dataset [28], myeloid cells were defined by combining the Macrophages and Neutrophils clusters; T cells were defined by combining CD4_Tcells, CD8_Tcells, and Treg clusters; and others were defined by combining NK and plasmacytoid_DCs clusters. The melanoma dataset GSE120575 was used to assess LAIR1 in responders versus nonresponders [29].

Digital spatial profiling

Freshly cut sections were first confirmed to contain adequate RNA quality using RNAscope LS 2.5 Probe Hs-PPIB (Advanced Cell Diagnostic, 313908). Adjacent tissue sections were then subjected to a whole transcriptome assay using guidelines from the manufacturer (GeoMx Human Whole Transcriptome Atlas; manual reference MAN-10115–05). Briefly, slides were deparaffinized and rehydrated in DEPC-treated water before being subjected to antigen retrieval using Tris-EDTA pH 9. Antigen retrieval was performed for 15 minutes at 99°C in a steamer using prewarmed buffer, and slides were then washed in PBS at room temperature for 5 minutes. Slides were then transferred to a 1 ug/mL proteinase K in PBS solution prewarmed to 37°C and incubated for 15 minutes, then washed in PBS for 5 minutes, and finally postfixed in 10% neutral buffered formalin (NBF) for 5 minutes. Slides were then washed twice in NBF stop buffer, and once in PBS. Slides were wiped and 200 μL hybridization solution was then applied. Hybridization was allowed to proceed overnight at 37°C for 16 hours. After hybridization, slides were subjected to 2 stringent washes at 25 minutes each at 37°C, then washed twice in 2X SSC buffer. Cells were then blocked with Buffer W at room temperature for 30 minutes in the dark, then subjected to staining with the morphology panel for 1 hour in the dark at room temperature. The morphology panel consisted of Syto-13 (ThermoFisher, S7575), anti-smooth muscle actin A488 clone 1A4, anti-pan cytokeratin A594 clone AE-1/AE-3, and anti-CD68 A647 clone KP1. Slides were then washed twice in 2X SSC and immediately transferred to the GeoMx instrument for stromal and tumor nest ROI selection. CD68+ cells were masked within these ROIs, and 8 um-wide contour-based TME masks spaced 2 μm away from the edge of the CD68 masks were then applied using ImageJ. Probes from all masks were collected and subjected to library preparation and subsequent sequencing using an Illumina HiSeq 4000. FASTQ files were then processed into DCC files using GeoMx NGS pipeline implemented at NGM. Data was then imported into the GeoMx instrument, background corrected, scaled, Q3-normalized, then exported as linear counts for analysis. Ingenuity pathway analysis

(Qiagen) was performed on DEGs, and pathways with Z-scores or bias corrected Z-scores > 2 and p values < 0.05 considered relevant.

Surface plasmon resonance

The ability of NGM438 to bind to recombinant human LAIR1-his and cynomolgus monkey LAIR1-his proteins was evaluated using surface plasmon resonance (SPR, Biacore, GE Healthcare Life Sciences) at 25°C. NGM438 was captured on flow cell 2, 3 and 4 of an anti-human Fc (fragment crystallizable region of antibody) capture surface. LAIR1-his proteins were injected at different concentrations (0.82 nM - 200 nM, 3-fold dilutions) onto all flow cells (flow cell 1 used as a reference surface) at a high flow rate (30 μL/min). Captured proteins were removed by injecting 3M MgCl2 for 30 seconds. The above experiment was also repeated on a Protein-A chip surface under similar conditions. Raw binding data were fitted to a 1:1 Langmuir binding model using BiaEvaluation software to calculate binding parameters, including KD (binding dissociation constant). Each experimental surface was carried out in triplicate (on three different flow cells with different NGM438 capture levels) for a total of n=6 data sets. NGM438 binding characteristics to human and cynomolgus monkey LAIR2, as well as rodent LAIR1, were evaluated in a similar manner. Rodents do not have a LAIR2 gene and therefore binding to rodent LAIR2 could not be assessed.

LAIR1-GFP reporter assays

The ability of anti-LAIR antibodies to antagonize the interaction between LAIR1 and collagen was evaluated using a flow cytometry-based reporter cell assay. Chimeric reporter cells were generated by fusing the ECD of human, cynomolgus monkey, or murine LAIR1 with the transmembrane and intracellular signaling domains of CD3ζ (cluster of differentiation 3 zeta chain). This LAIR1-CD3ζ construct was inserted into a retrovirus used for stable infection of a mouse T-hybridoma cell line containing a DNA element with a nuclear factor of activated T-cells (NFAT) promoter upstream of green fluorescent protein (GFP). In these reporter cells, NFAT signaling results in GFP expression that can be measured by flow cytometry. In some experiments, plates were coated overnight at 4°C in PBS with 1μg/mL human collagen type 1 or 1 μg/mL human collagen type 4. In separate experiments, plates were prepared with 4mg/mL polymerized collagen matrix. Collagen matrix was prepared on ice using high concentration rat tail collagen and 50mM HEPES in RPMI 1640 and 10% heat-inactivated fetal bovine serum (FBS) and solidified on 96-well plates at 37°C. In separate experiments, BEND3 (ATCC) tumor cells expressing collagens were added to plates. Antibodies were added in a dose titration prior to addition of reporter cells in RPMI 1640 and 10% heat-inactivated FBS, and the mixture was incubated at 37°C overnight. GFP expression was measured by flow cytometry (LSRFortessa, BD Biosciences) and analyzed by FlowJo (BD Biosciences). GFP+ cells were defined by comparing the gates of uncoated wells vs. wells coated with an anti-LAIR1 mAb positive control. Each experiment was carried out three or more independent times.

Collagen-driven myeloid reprogramming

Dendritic cells were derived from monocytes, which were purified from PBMCs using a human pan monocyte isolation kit (Miltenyi). DCs were generated by culturing monocytes in X-VIVO 15 media (Lonza) containing 50 ng/mL recombinant human GM-CSF

(Peprotech) and 50 ng/mL recombinant human IL-4 (Peprotech) for 5–6 days. 96-well tissue culture plates (Corning) were coated with 5 μg/mL human collagen type 1 (Millipore Sigma) in PBS overnight at 4° C, then washed in PBS. 1×10^5 DCs were added to the plates with anti-LAIR1 or an isotype control antibody at the listed concentrations then incubated for 2 days at 37° C. Conditioned media was collected the next day and analyzed using Luminex (ProcartaPlex, ThermoFisher). RNA was also extracted and subjected to sequencing using the TailorMix Directional RNA Sample Preparation Kit (SeqMatic, TM200-A) and sequenced on an Illumina NovaSeq S1 (100 bp single-end reads; an average of 24 million reads were generated for each sample). To align sequences, raw reads were filtered via Trim Galore! in order to eliminate low-quality and adaptor bases, and reads less than 20 nucleotides were removed. Mapping of filtered reads to UCSC hg19 genome sequences was performed using STAR (v2.6.0a). Counts were created using featureCounts (v1.6.2), and edgeR (v3.22.3) was used to generate normalized counts and execute DEG analysis [30,31]. Volcano plots were generated using VolcaNoserR [32]. Top hits were ranked using Manhattan distance criterion. IPA was performed as described above. Experiments were performed using at least 3 independent donors.

Fc-receptor activation assay

96-well MaxiSorp (Nunc) plates were coated with 5 μg/mL human IgG1 antibody in the presence or absence of 1 μg/mL human collagen type 1 (Millipore Sigma) in PBS for 2 hours at room temperature followed by washing the plates in PBS. 7×10^4 monocyte-derived dendritic cells were added to the plates with the indicated antibodies at the listed concentrations, or 5 μg/mL for single dose experiments, and incubated overnight at 37° C. Supernatants were collected the next day and tumor necrosis factor alpha (TNFα) production was measured using Luminex (ProcartaPlex, ThermoFisher Scientific).

Collagen-skewed mixed lymphocyte reaction

Human T cells were purified from PBMCs using a human pan T isolation kit (Miltenyi). 96-well plates were coated with 5 μg/mL human collagen type 1 (Millipore Sigma) in PBS overnight at 4° C. The plates were then washed and 1×10^5 allogeneic pan T cells and 2.5×10^4 monocyte-derived dendritic cells and were added to each well with experimental antibodies. Cells were then incubated for 4–5 days at 37° C. Conditioned media was harvested for measurement of cytokine production by Luminex assay (ProcartaPlex system; ThermoFisher). To measure proliferation, fresh media containing tritiated thymidine ([3H]-thymidine; Perkin-Elmer) was added at a concentration of 1 μCi/mL. After an additional overnight incubation, cells were harvested on to filters using a Harvester96™ (Tomtec) and 3H-thymidine incorporation was counted on a MicroBeta2 microplate reader (PerkinElmer). NGM438, isotype control antibody (anti-KLH), and anti-PD-1 (pembrolizumab) were each used at 5 ug/mL final concentration.

Flow cytometry-human

To assess LAIR1 on circulating and intratumoral myeloid cells, matched blood and resected tumor samples collected on the same day from 15 patients diagnosed with various solid cancers. Circulating monocytes were assessed in PBMCs isolated from buffy coats. Briefly, blood samples were first diluted in 50 mL conical tubes with an equal amount of PBS

then gently mixed by inverting. Ficoll was added to new 50 mL tubes using 8 mL Ficoll for every 20 mL diluted blood. Diluted blood was then overlaid onto the Ficoll. Tubes were then centrifuged at room temperature at 350 x g for 30 minutes with the brake set to the off position. After density gradient centrifugation, buffy coats were removed, then washed 3 times in PBS. Intratumoral macrophages were assessed in matched tumor resections. Tumors were first dissociated using a tumor dissociation kit per the included instructions (Miltenyi; 130–095-929). Tumors were minced then subjected to mechanical and enzymatic digestion. Digested tumor was filtered through a 70 μm strainer then washed 3 times in PBS with BSA. Cells were then suspended in PBS. PBMC and dissociated tumor were both stained with 1X Live Dead Fixable Violet Dead Cell Dye in PBS (ThermoFisher, L23105), washed, then suspended in 1X Fc Block buffer and incubated on ice for 30 minutes. A master mix cocktail containing anti-CD45 PE-CF594 clone HI30, anti-CD14 BUV805 clone M5E2, anti-CD15 BV786 clone H198, anti-CD11b BV650 clone M1/70, and anti-LAIR1 BUV395 clone DX26 was then applied to the Fc Blocked-cells and the mixture was allowed to incubate for 30 minutes on ice. Cells were washed twice and measured by flow cytometry using an LSRFortessa (BD Biosciences) and analyzed by FlowJo (BD Biosciences). Statistical analysis was performed using a paired T-test between the LAIR1 geoMFI on gated peripheral monocytes and tumor-infiltrating macrophages (Graphpad Prism). For assessment of LAIR expression between NHD and CPI, and NGM438 occupancy, blood was procured from Discovery Life Sciences (CPI) and Innovative Research (NHD). 4 mL blood from each donor, was mixed with 160 mL red blood cell lysis buffer (1% ammonium chloride) and incubated in the dark for 15 minutes, inverting the mixture every 3 minutes. This was then divided into 50mL conical tubes and centrifuged for 20 min at 500 x g at ambient temperature. Cells were resuspended in 10 mL stain buffer, and pipetted into a 15 mL conical tube, then centrifuged at 500 x g at ambient temperature. Cells were resuspended in 4 mL 1X Live Dead Fixable Blue Dead Cell Dye and incubated in the dark on ice for 20 minutes. Cells were then washed in phosphate-buffered saline (PBS) twice and resuspended in 2 mL 2X fragment crystallizable (Fc) block and aliquoted in a 96 well plate and incubated at room temperature for 10 minutes. A 1:4 dilution series of NGM438 covering 8 dilutions and starting at 15 μg/mL was then applied to the plate and incubated for 30 minutes at room temperature, followed by the addition of a master mix of antibodies (anti-CD45 APC-H7 clone 2D1, anti-CD3 PE-Cy7 clone SK7, anti-CD33 PE clone WM53, anti-CD19 BUV805 clone SJ25C1, anti-CD8 BUV395 clone RPA-T8, anti-HLADR BV711 clone L243, anti-CD15 BV605 clone W6D3, anti-CD56 BV421 clone 5.1H11), NGM438-competing antibody (clone 62G10 labeled with AlexaFluor 647), and NGM438-noncompeting antibody (clone 57D12 labeled with AlexaFluor 488) then incubated at room temperature in the dark for 30 minutes. Cells were washed twice, fixed in Fluorofix for 30 minutes at room temperature, then washed. Cells were then acquired by flow cytometry using an LSRFortessa (BD Biosciences) and analyzed by FlowJo (BD Biosciences). LAIR1 expressing cells were gated using NGM438 non-competing antibody clone 57D12 fluorescence signal. LAIR1 expression was calculated from the competing antibody (clone 62G10) using a four parameter least squares fit with variable slope equation (Graphpad Prism) of background-subtracted geometric mean fluorescence intensity (geoMFI) values. Total endogenous LAIR1 expression was interpreted as the geoMFI at which LAIR1 was completely unoccupied, defined as the upper signal

plateau at lowest NGM438 concentrations, resulting in maximal signal from the competing antibody from each donor (i.e. best-fit top values).

Cell based binding studies

The ability of NGM438 to bind cells expressing LAIR1 was evaluated using flow cytometry. In one set of experiments, 293T cells were transiently transfected with plasmids expressing full length human and cynomolgus monkey LAIR1 using lipofectamine 2000 transfection reagent (according to the manufacturer's instructions). Additional cells were transfected with a plasmid expressing a truncated human LAIR1 isoform with a 17 amino acid ECD deletion (Accession# Q6GTX8–2, also known as "isoform 2"). Transfected cells were washed in phosphate buffered saline (PBS) staining buffer containing 1% bovine serum albumin (BSA) and 0.1% sodium azide. Cells were then stained with a concentration range of NGM438 or isotype control antibody (anti-keyhole limpet hemocyanin, KLH) that matched the Fc region of NGM438 for 30 minutes at room temperature, then washed and stained with fluorescent anti-human Fc secondary antibody for 30 minutes at 4°C. Cells were washed again followed by detection using flow cytometry (IntelliCyt, Sartorius). An additional set of cells expressing stable full-length ECD of human and cynomolgus monkey LAIR1 were also evaluated for NGM438 binding. Each experiment was carried out in triplicate.

Murine tumor experiments

The murine lung cancer cell line 344SQ was derived from *K-ras*$^{LA1/+}$*p53*$^{R172H\Delta g/+}$ mice as previously described [33]. 6–8 week old 129/Sv mice were obtained from Charles River Laboratories. For studying the tumor growth in syngeneic immunocompetent models, 344SQ cells (1×10^6) were implanted subcutaneously into the right flank of male and female mice. When tumors reached an average size of 50–100 mm^3 anti-LAIR was dosed 10 mg/kg I.P. twice per week and/or anti-PD-1 (Bioxcell) was dosed 8 mg/kg once per week. Tumor growth was measured with digital calipers once a week, and tumor sizes were calculated using the formula: ½(length × width × width) at indicated time points. At end points, mice were sacrificed to examine the tumor weight and metastatic lung nodules as described previously [34]. GEMM ($Kras^{LSL\text{-}G12D}/p53^{fl/fl}$) were generated as previously described [33,35]. Mice were infected at 3–4 months of age with 2.5×10^7 titer pfu adenovirus-cre by intratracheal intubation. Treatment with antibodies were performed at 2 months post-infections when tumors were visualized by micro-CT imaging. All mice were immunocompetent and assessed for health daily by the department of veterinary medicine and surgery at The University of Texas MD Anderson Cancer Center. All animal procedures were reviewed and approved by The University of Texas MD Anderson Cancer Center Animal Care and Use Committee.

Immunohistochemistry on murine tumors

Paraffin-embedded 344SQ tumors were processed following standard protocols. Primary antibodies are listed in Table S1. TUNEL assay kit from Abcam was used following manufacturer instructions. Quantitation of images was performed using ImageJ–colour deconvolution plugin and 8–10 FOV per tumor were used with 5 tumors per treatment group. IHC for collagen I and Iba1 was performed using a Bond Polymer Refine Detection

kit on the Leica Bond Rx autostainer, which included dewaxing, heat-induced epitope retrieval, antibody incubation, signal detection, and hematoxylin counterstaining. Collagen I was detected using anti-collagen clone (E8F4L) XP® Rabbit mAb #72026 from Cell Signaling, and Iba1 was detected using clone (E4O4W) XP® Rabbit mAb #17198 from Cell Signaling. Slides were removed from the autostainer, rinsed in water, dried, and cover slipped using Surgipath MM 24 Mounting Media.

Flow cytometry-murine

Tumors were processed following the MACS (Miltenyi) mouse tumor dissociation kit. Tumors were chopped into 2–3 mm fragments and then placed in digestion media. Mechanical dissociation using the gentleMACS Octo dissociator (Miltenyi) was followed with incubation at 37°C. RBC lysis buffer (BioLegend) was added to tumor cell suspension following manufacturer recommendation. Tumor cell suspensions were incubated with anti-CD16/CD32 to block non-specific binding and then stained for 1 hr at room temperature with mixture of cell surface fluorochrome conjugated antibodies. For intracellular staining cells were fixed and permeabilized using BD Cytofix/cytoperm buffer (BD Biosciences). Cells were then stained with mixture of intracellular mixture of fluorochrome conjugated antibodies for 1 hr. The stained cells were acquired on a Cytek Aurora and the data analyzed using FlowJo software. Single color references were validated before running the panel and spectral unmixing performed.

Murine tumor RNA sequencing

Total RNA from tumors was isolated using Trizol and was purified using an RNAeasy kit (Qiagen). Total RNA was then prepared for sequencing using the TailorMix Directional mRNA sample preparation kit (SeqMatic) and sequenced on an Illumina NovaSeq SP (100 bp single-end reads and an average of 40 million reads were generated for each sample). For sequencing alignment, RNA-seq data raw reads were filtered using Trim Galore! to remove low quality and adaptor bases. Reads shorter than 20 nt were discarded. Filtered reads were mapped to UCSC mm10 genome sequences using STAR (v2.7.6). Counts of all samples were generated using featureCounts (v2.0.1), and edgeR (v3.40.1) was used to get normalized counts and perform differential gene expression analysis [30,31,36,37].

Data availability

The data generated in this study are available within the article and its supplementary data files or upon request from the corresponding authors. Expression profile data analyzed in this study were obtained from Gene Expression Omnibus (GEO) at GSE114725, GSE178341, GSE121861, GSE119352, Genome Sequence Archive (GSA) at CRA001160, and The Broad Institute Single Cell Portal (SCP) at SCP1288. The sequence data generated in this study are publicly available in Gene Expression Omnibus (GEO) at GSE260596, GSE260597, GSE260598.

RESULTS

LAIR1 expression is associated with stroma abundance and is enriched in tumor-associated myeloid cells

Cancer-immune phenotypes are believed to reflect distinct inhibitory mechanisms that limit anti-tumor immune response [38]. Thus, to gain insight on the role of LAIR1 in cancer, we assessed LAIR1 within the context of immune desert, excluded, and inflamed tumors using pathologist-scored sections from head and neck squamous cell carcinoma (HNSCC). LAIR1 expression was detected within all immune phenotypes and was observed primarily in regions with high immune cell infiltration (Fig. 1A). Interestingly, the distribution of LAIR1 also favored stromal tracks, which suggested LAIR1/collagen engagement was a feature of stroma-rich cancers (Fig. 1A). To probe the generality of this association, we first expanded our histological assessment to include samples from pancreatic ductal adenocarcinoma (PDAC), non-small cell lung cancer (NSCLC), and renal cell carcinoma (RCC). Indeed, LAIR1-expressing cells were enriched within collagen-rich, picrosirius red (PSR)-stained, stromal areas across all indications (Fig. 1B). We then assessed *LAIR1* gene expression in the top and bottom ECM quartiles across 31 solid tumor indications within The Cancer Genome Atlas (TCGA) using an ECM gene set identified in TGFβ-activated fibroblasts [20]. *LAIR1* expression was significantly higher in the top ECM quartiles in 25 of the 31 indications (Fig. 1C).

Given the link between tumor stroma and immune suppression, we next asked whether this suppression could be mediated by specific $LAIR1^{+}$-immune cell subsets. We first assessed FACS-based LAIR1 expression on circulating cells from 10 normal healthy donors (NHD) and 9 cancer patients actively receiving checkpoint inhibitor therapy (CPI; Fig. S1; Table S2). LAIR1 was detected on every immune subset in all cases, with no change in the level of LAIR1 expressed on cells from NHD versus CPI patients. We then examined *LAIR1* gene expression in tumors using publicly available human scRNA-seq datasets for RCC, NSCLC, PDAC, colorectal carcinoma (CRC) and breast carcinoma (BRCA) [21–26]. As LAIR1 has been reported to mediate both T cell and myeloid suppression, we categorized clusters into 3 groups: T cells, myeloid, and non-T/myeloid (Fig. 1D). Myeloid cells represented most LAIR1-expressing cells across all tumor types, with similar results observed in 2 scRNA-seq datasets derived from mouse tumors (Fig. 1E; [27,28]). We then asked if myeloid-expressed LAIR1 could be regulated by the tumor microenvironment (TME). For this we compared FACS-based LAIR1 expression on CD15-CD14+CD11b+ myeloid cells from PBMC to their matched counterparts in dissociated tumor samples across 15 patients diagnosed with either ovarian cancer (OV), RCC, or PDAC (Fig. 1F; Table S3). Indeed, tumor associated myeloid cells expressed significantly more LAIR1, suggesting LAIR1-mediated myeloid suppression can be augmented by the TME. Altogether, our results demonstrate that LAIR1 expression is correlated with tumor stroma and most strongly reflects myeloid content.

The stromal TME elicits a suppressive myeloid phenotype

We hypothesized LAIR1 expression was such that stroma-associated myeloid cells represented a major source of immune-suppression in tumors, likely via LAIR1/collagen engagement. Therefore, we used digital spatial profiling to compare the transcriptome

of myeloid cells residing in stroma-rich TMEs to counterparts residing in stroma-free tumor nests in OV, NSCLC, and gastric cancer biopsies. Stroma-associated myeloid cells (SAM) were defined as CD68+ cells coincident with alpha-smooth muscle actin (α-SMA+) regions of interest (ROI), while tumor nest-associated myeloid cells (TNAM) were defined as CD68+ cells coincident with pan-cytokeratin-rich ROIs devoid of α-SMA (Fig. 2A). To address potential contamination from adjacent cells, we identified TME genes using a TME mask to capture transcripts from cells immediately surrounding CD68+ myeloid cells (Fig. 2A and S2A). Transcripts identified as TME were then removed from the gene lists derived from CD68+ SAM or TNAM, leaving behind genes that were specifically expressed by each myeloid compartment (Fig. 2A). To confirm our approach for identifying myeloid-expressed genes, we compared expression of *CD68*, *CD14*, *CSF1R*, *FCER1G*, *LYZ* and *LAIR1* across SAM, TNAM, and both TMEs. Indeed, SAM and TNAM expressed significantly higher levels of each gene compared to either TME (Fig. 2B). Importantly, we found no change in the level of expression of these genes between SAM and TNAM, confirming the myeloid nature of both compartments. Further, ECM-related gene expression was significantly elevated in stromal TMEs compared to tumor nest TMEs, while tumor nest TMEs expressed significantly higher epithelial gene expression, confirming our selection of stromal and tumor nest ROIs (Fig. S2B). Subsequent differential gene expression analysis performed on SAM and TNAM identified 50 differentially expressed genes (DEGs) that were significantly elevated in TNAM and 128 DEGs that were significantly elevated in SAM (Fig. 2C).

To identify phenotypic differences reflected by these genes, all 178 DEGs were subjected to Ingenuity Pathway Analysis (QIAGEN Inc., https://www.qiagenbioinformatics.com/products/ingenuitypathway-analysis;[39]. Indeed, canonical pathway analysis revealed chemokine signaling, dendritic cell maturation, and calcium-induced T cell apoptosis to be increased in SAM while MSP-RON signaling was increased in TNAM (Fig. 2D). Further, SAM and TNAM were associated with distinct disease or biological functions, where SAM DEGs favored development of phagocytic antigen presenting cells (APCs) and TNAM DEGs favored proliferation and infiltration (Fig. 2D). Strikingly, this analysis predicted INHBA, a TGFβ superfamily member reported to promote an inflammatory myeloid phenotype, as an upstream regulator of TNAM, and IL-10, TGFβ1, IL-4, and RICTOR, known drivers of anti-inflammatory phenotypes in myeloid cells, as upstream regulators of SAM, highlighting the stroma as a suppressive TME (Fig. 2D). Indeed, compared to the TNAM, SAM expressed significantly higher levels of *F13A1*, *STAB1*, *CD163*, *MRC1*, *FOLR2*, *CCL8*, *CCL2,* genes known to be expressed by suppressive anti-inflammatory myeloid cells (Fig. 2E). Conversely, SAM expressed significantly lower levels of the interferon-induced genes *IFI6* and *IFIT1,* as well as *ALDOA,* the gene product for which is critical for glycolysis, a key feature of inflammatory myeloid cells (Fig. 2E). Interestingly, SAM also expressed significantly higher levels of *ADAM19*, *RCN3*, and *WIPF1*, and lower levels of *JUP* and *PDLIM1*, genes whose products could potentially influence the stroma-myeloid dynamic via modulation of cell-cell or cell-ECM interactions (Fig. 2E; [40–44]).

We reasoned that if LAIR1/collagen signaling was indeed a driver of the SAM phenotype, LAIR1 gene expression would correlate with that of the SAM gene set in human tumors. To test this concept, we utilized TCGA data to conduct Pearson correlation of LAIR1 with

the aggregate SAM gene set sum in LUSC, OV, and stomach adenocarcinoma (STAD). We observed strong correlation between LAIR1 and SAM genes across all indications, with r = 0.8672 in LUSC, 0.6807 in OV, and 0.7129 in STAD (Fig. 2F). This contrasted with poor correlations observed between LAIR1 and the aggregate TNAM gene set sum, a finding that suggests LAIR1 is not required for the TNAM phenotype. Altogether, our results demonstrate that tumor stroma drives a novel suppressive myeloid phenotype that correlates highly with LAIR1 expression in human cancer.

Development of NGM438, a novel antagonist of LAIR1 and collagen engagement

We hypothesized that LAIR1/collagen engagement polarized SAM towards an immunosuppressive phenotype and that blocking this interaction would promote anti-tumor immune responses. Accordingly, we developed NGM438, a humanized IgG1 effector-less monoclonal antibody that binds LAIR1 and antagonizes the LAIR1/collagen interaction (for sequence and preparation details see examples 3 and 4 in PCT/US2021/038251; [45]). We assessed the binding affinity of NGM438 to LAIR1 using surface plasmon resonance (SPR) and found it to bind with high affinity to both human (K_D = 0.26 ± 0.03 nM) and cynomolgus monkey (K_D = 4.28 ± 0.66 nM) LAIR1 (Fig. 3A; Table S4). NGM438 failed to bind human LAIR2 as well as LAIR1 from mouse or rat. We also confirmed binding to LAIR1 expressed on cells as summarized in Table S5.

We next assessed the ability of NGM438 to disrupt LAIR1/collagen engagement using chimeric LAIR1 reporter cells that expressed a LAIR1-CD3ζ fusion protein. Here, activation of the chimeric receptor by collagen results in Nuclear Factor of Activated T cells (NFAT)-driven green fluorescent protein (GFP) expression. We exposed this reporter to diverse collagens including purified human collagens I and IV, polymerized rat tail collagen, and collagens expressed on the surface of mouse BEND3 cells, while including increasing concentrations of NGM438 or an isotype control antibody. In this cell-based assay, NGM438 potently suppressed collagen-induced GFP expression in all cases (Fig. 3B).

We then asked whether blocking LAIR1/collagen engagement with NGM438 could skew the phenotype of collagen-experienced myeloid cells using clone 47H1, the parental antibody that shares its complementarity-determining regions (CDRs). For this, we cultured IL-4/GM-CSF-differentiated monocyte-derived dendritic cells (moDC) on collagen-coated surfaces in the presence of either 47H1 or an isotype control antibody, then performed RNA sequencing and subsequent DEG analysis. Indeed, using 1.5-fold change and $p < 0.05$ as cut-offs, we identified 420 DEGs induced by LAIR1/collagen blockade, and 507 DEGs repressed (Fig. 3C). Further, 47H1 repressed 21 of the 128 SAM genes identified in stromal ROIs, which included suppressive genes such as *CD163*, *F13A1*, *CCL13*, *STAB1*, and *FOLR2* (Figs. 2C and 3C). In contrast, 3 TNAM genes, *SPP1*, *CXCL8*, and *MMP12*, were identified as DEGs and were each induced by 47H1 (Fig. 3C). We then subjected all DEGs to IPA and found LAIR1/collagen blockade to be associated with disease and biological functions involved in tumor regression such as inhibition of tumor growth, proliferation, and activation of tumor cell death and apoptosis, as well as activation of phagocytes (Fig. 3D). Further, upstream regulator analysis predicted activation of several pro-inflammatory stimuli, including lipopolysaccharide, tetradecanoylphorbol acetate (TPA), TREM1, and

5-O-mycolyl-beta-araf-(1->2)-5-O-mycolyl-alpha-araf-(1->1')-glycerol (Mma_DMAG), and inhibition of anti-inflammatory molecules including aflatoxin B and PTGER2 (Fig. 3E).

Results from the DEG analysis indicate LAIR1/collagen engagement can directly regulate myeloid inflammatory status, therefore we next asked whether collagen itself induced this inflammatory switch in the presence of LAIR1-blockade. For this, we measured secretion of 3 inflammatory molecules identified among the top hits in the DEG analysis: CCL3, CCL4, and IL1RN (Fig. 3F). When cultured on collagen coated-surfaces, moDC responded to LAIR1/collagen blockade with robust and dose-dependent secretion of all 3 proteins; however, neither NGM438 nor 47H1 elicited any response by moDC cultured on uncoated surfaces (Fig. 3F). Thus, NGM438 unlocks collagen-dependent suppression of myeloid inflammation by blocking LAIR1/collagen interactions. We next asked whether LAIR1/collagen-blockade could reverse collagen suppression of inflammatory signaling transduced by molecules other than collagen. To address this, we tested the ability of NGM438 to reverse collagen-suppressed Fc-receptor (FcR) activity in moDC. Indeed, NGM438 completely blocked collagen's ability to inhibit FcR-driven TNFα secretion (Fig. 3G).

Given that LAIR1 can also regulate activation of non-myeloid lineage cells, we hypothesized NGM438 will reverse suppression beyond the stromal myeloid compartment in patients. Accordingly, we tested NGM438's ability to bind to LAIR1 expressed on peripheral immune cells using a LAIR1 receptor occupancy (RO) assay. Indeed, NGM438 competed with our LAIR1-detection antibody with a similar IC_{50} across all immune subsets including NK cells, B cells, T cells, NKT cells, and monocytes, in blood from both NHDs and cancer patients (Fig. 3H). Altogether, these data demonstrate LAIR1 regulates suppression of both collagen-stimulated and FcR-stimulated myeloid inflammation and identify NGM438 as a novel antagonist of this suppressive axis with broad immune-stimulating potential.

LAIR1 is associated with resistance to checkpoint inhibition

We next explored whether blockade of LAIR1/collagen engagement could enhance T cell activation using a modified mixed-lymphocyte reaction (MLR), where moDC stimulators are mixed with allogeneic pan-T cell responders in the presence of collagen. Here collagen significantly suppressed moDC-driven T cell proliferation (Fig. 4A). Indeed, LAIR1/collagen blockade with 47H1 reversed the suppressive effect of collagen in a dose-dependent fashion (Fig. 4A). Given that LAIR1/collagen engagement and the PD-1/PD-L1 axis are distinct mechanisms of suppression, we hypothesized that simultaneous inhibition of both would have additive or synergistic effects on T cell proliferation. We therefore tested NGM438 in combination with anti-PD-1 in the collagen-suppressed MLR assay. Interestingly, we were unable to identify donor pairs that responded to anti-PD-1 alone; however, we identified two patterns of synergy: one where NGM438 elicited single agent activity that was significantly enhanced by anti-PD-1, and one where NGM438 was inactive alone but elicited robust proliferation in combination with anti-PD-1 (Fig. 4B). In line with these results, the combination induced IFNγ, IL-2, and TNFα secretion to levels above that observed with either single agent (Fig. 4C). Thus, LAIR1/collagen blockade with NGM438 can enable response to PD-1 inhibition in otherwise PD-1 refractory conditions.

Given the association of LAIR1 with resistance to anti-PD-1 *in vitro*, we reasoned that LAIR1 may be associated with resistance to immune checkpoint inhibition in cancer patients. We therefore assessed *LAIR1* expression in a melanoma scRNA-seq dataset generated from patients that were either refractory or went on to respond to anti-CTLA4, anti-PD-1, or combination anti-CTLA4 plus anti-PD-1 [29]. *LAIR1* transcripts were detected in a minority of T cells, B cells, and plasma cells, but were present in most dendritic cells (DCs) and macrophages (Fig. 4D). We then compared *LAIR1* expression between non-responders and responders, focusing on populations that contained at least 10% *LAIR1*-expressing cells. Strikingly, *LAIR1* expression in macrophages was significantly higher in non-responders compared to responders (Fig. 4E). Overall, our results support the concept of LAIR1-mediated resistance to checkpoint inhibitor therapy.

LAIR-1 blockade sensitizes metastatic collagen-rich Kras/p53 mutant NSCLC tumors to anti-PD-1 therapy

Given our results, we hypothesized that NGM438 would sensitize anti-PD-1 refractory tumors that contained high levels of coincident stroma and myeloid cells. Accordingly, we developed a mouse LAIR1-reactive NGM438-surrogate antibody (clone 43H2) and tested this in a collagen and myeloid rich, anti-PD-1 refractory immunocompetent syngeneic tumor model of Kras/p53 (KP) mutant NSCLC (Fig. S4A) [46,47]. The KP 344SQ line was previously found to have collagen-induced T cell exhaustion mediated through LAIR1 [4]. We evaluated LAIR1 on immune cells in the KP 344SQ model and found high LAIR1 expression on myeloid subsets (macrophage, neutrophils, and dendritic cells) making this model suitable to evaluate efficacy of NGM438-surrogate (Fig. 5A). Mice bearing the KP tumors were treated with either anti-LAIR1, anti-PD-1, or combination anti-LAIR1/anti-PD-1. We found that dual LAIR1/PD-1 blockade significantly reduced both primary and metastatic tumor burden compared to either single agent alone (Fig. 5B–C). Further, histological analysis of primary tumors revealed the combination increased the prevalence of apoptotic cells as measured by TUNEL staining, and decreased proliferation as measured by Ki67 (Fig. 5D). In addition, we also evaluated CD8 and granzyme-B expression in the primary tumors and found increased CD8/granzyme-B in the anti-LAIR1/anti-PD-1 group (Fig. 5E). Given NGM438's ability to reprogram suppressive myeloid cells and restore collagen-suppressed T cell proliferation, we next explored the impact of clone 43H2 on tumor-associated immune cells using multi-spectral flow cytometry at early (week 2), middle (week 3) and late (week 4) treatment time points. Indeed, CD8+ T cell content trended upwards in the combination group at weeks 2 and 3 and reached statistical significance above both single agents by week 4 (Fig. 5F). The anti-LAIR1/anti-PD1 combination also increased the frequency of both effector/memory and granzyme B+ CD8+ T-cells, and concomitantly decreased CD8+ T cells expressing exhaustion markers (Fig. 5F, Fig. S4B). Interestingly, CD8+ T cell activation was preceded by a significant increase in iNOS+ MHCII-high macrophages at week 2 that was not apparent at weeks 3 or 4 (Fig. 5F). To better understand the nature of the reversal of LAIR1/collagen-driven resistance to anti-PD-1 in this model, we compared gene expression in tumors from mice treated with combination anti-LAIR1/anti-PD-1 to those treated with anti-PD-1 alone (Fig. 5G). We identified 36 DEGs and subjected these to IPA upstream regulator analysis, which predicted activation of several pro-inflammatory stimuli, and inhibition of several anti-inflammatory

stimuli, highlighting reversal of immune suppression induced by the NGM438 surrogate (Fig. 5H). In line with this, many of the DEGs we identified were known interferon-induced genes including, *Ccl8*, *Cxcl9*, *Cxcl10*, *Cxcl11*, *Mx1*, *Ifi44*, *Ifit1*, *Gbp3*, *Gbp4*, and *Gbp5* (Fig. 5I). In addition, we evaluated the combination of LAIR1/PD-1 blockade in the autochthonous lung cancer GEMM ($Kras^{LSL\text{-}G12D}/p53^{fl/fl}$) where tumors were induced via intratracheal administration of adenoviral-Cre recombinase [18,48]. Primary lung tumors developed after 8 weeks and tumors were confirmed by micro-CT imaging (Fig. 5J, left). Mice with lung tumors were randomized and treated with anti-LAIR1 or anti-LAIR1/-PD-1 for 8 weeks (Fig 5J, right). Micro-CT images analysis indicated that mice treated with anti-LAIR1/-PD-1 had a decrease percentage change of tumor burden compared to mice treated with LAIR1 blockade alone. H&E-stained lung sections at week 8 show a lower total number of tumors as well as a smaller tumor size in the combination treatment group (Fig. 5K). Altogether, these results support the notion that LAIR1/collagen engagement acts as a resistance mechanism to anti-PD-1 therapies.

DISCUSSION

In the current study we show that LAIR1 is heavily compartmentalized in cancer, predominately expressed by myeloid cells, most of which are associated with tumor stroma. LAIR1 is hypothesized to function as a sensor, transducing suppressive signals in the context of collagen-rich microenvironments [49,50]. The co-distribution of LAIR1 and stroma, which consists largely of collagens, suggests to us that such suppression could be a general feature of stroma and likely contributes to its tolerogenic nature [51,52]. This notion is supported by our finding that myeloid cells residing in stromal niches, aka SAM, exhibit a phenotype distinct from their non-stroma associated counterparts, characterized by enhanced expression of M2-associated genes, reduced expression of interferon-inducible genes, and an overall gene expression profile resembling IL-10-, TGFβ1-, and IL-4-driven polarization. Further, we identified a gene set enriched in SAM, and found that LAIR1 prevalence in tumors was associated with high SAM gene expression, implicating the LAIR1/collagen axis in the acquisition of the SAM phenotype.

Myeloid cells represent the most abundant immune cell subset in cancer and are thought to promote tumor progression in part through suppression of anti-tumor immunity [53]. Here, we extend this and add that these cells are a major source of intratumoral LAIR1. LAIR1 thus integrates ECM and myeloid-derived immunosuppression, making LAIR1/collagen blockade an attractive strategy for evoking myeloid-regulated anti-tumor immune responses in stroma-rich cancers. We therefore developed NGM438, a first in class anti-LAIR1 monoclonal antibody that blocks LAIR1/collagen engagement. Indeed, NGM438 skewed collagen-experienced myeloid cells towards an inflammatory phenotype and unlocked both collagen-driven and FcR-driven myeloid inflammation *in vitro.* As NGM438 activity was characterized by chemokine secretion, we predict NGM438-reprogrammed myeloid cells may induce T cell infiltration in tumors. Further, our results demonstrate that collagen limits inflammation via LAIR1, a finding that suggests ECM abundance will augment NGM438 activity such that stroma-rich cancers may favor response.

Though immune checkpoint inhibition represents a breakthrough in cancer treatment, many patients either fail to respond or go on to develop resistance [1]. Recently, ECM gene expression was found to be higher in tumors from checkpoint therapy refractory patients compared to those from patients that went on to respond, observations that established a link between ECM and resistance to checkpoint inhibition [3]. In line with this idea, we previously reported ECM gene expression was higher in anti-PD-1 treated melanoma patients that developed progressive disease compared to those that showed partial or complete response, while LAIR1 expression was associated with reduced survival [4]. These results supported the idea that LAIR1/collagen engagement acts as a resistance mechanism, but they did not address the identity of the LAIR1 compartment due to the cellular heterogeneity represented in the material used for analysis. In the current study we analyzed single cell gene expression data and found LAIR1 expression was more abundant in macrophages, and not T cells, from refractory melanoma patients compared to their counterparts from responding patients. These results further support our hypothesis that collagen and LAIR1-expressing myeloid cells act together to drive immunosuppression in the tumor microenvironment which contributes to checkpoint inhibitor resistance. This idea is supported by our finding that NGM438 could induce myeloid inflammation and synergize with anti-PD-1 *in vitro*. These data suggest that NGM438 may be able to address the significant unmet need created by both intrinsic and acquired resistance.

Our data further highlight the potential of targeting the LAIR1/collagen axis in patients diagnosed with solid cancers. We and others previously found that forced expression of LAIR2, a soluble LAIR1 antagonist that competes with LAIR1 for collagen binding, could synergize with anti-PD-1 in a refractory model of lung cancer [4]. TNC410, a LAIR2-hIgG1 Fc fusion protein proposed to antagonize LAIR1 in the manner, is currently undergoing clinical development in solid tumor indications (NCT05572684). NGM438 utilizes a distinct mechanism of inhibition compared to NC410, binding directly to LAIR1 to block immune-suppressive LAIR1/collagen signaling. We generated a mouse reactive NGM438 surrogate antibody and found that specific inhibition of LAIR1/collagen synergized with anti-PD-1 to block tumor growth in multiple murine models by mobilizing intratumoral inflammation. NGM438 is currently being assessed in a phase 1 clinical trial for solid tumor indications as monotherapy and in combination with anti-PD-1 (NCT05311618).

Supplementary Material

Refer to Web version on PubMed Central for supplementary material.

Acknowledgements:

We thank the members of our laboratories for critical discussions.

Funding:

This work was supported in part by CPRIT RP200235, CPRIT-MIRA RP160652-P3, Rexanna's Foundation for Fighting Lung Cancer, the Connie Rasor Endowment for Cancer Research, and NCI P50CA070907 to D.L.G. D.L.G. holds the Isaiah J. Fidler Professorship in Cancer Research. The work was also supported by the generous philanthropic contributions to The University of Texas MD Anderson Lung Cancer Moon Shots Program and the MD Anderson Cancer Center Support Grant (CCSG P30CA016672).

References

1. Sharma P, Hu-Lieskovan S, Wargo JA, Ribas A. Primary, Adaptive, and Acquired Resistance to Cancer Immunotherapy. Cell 2017;168(4):707–23 doi 10.1016/j.cell.2017.01.017.
2. Keerthivasan S, Şenbabaoğlu Y, Martinez-Martin N, Husain B, Verschueren E, Wong A, et al. Homeostatic functions of monocytes and interstitial lung macrophages are regulated via collagen domain-binding receptor LAIR1. Immunity 2021;54(7):1511–26.e8 doi 10.1016/j.immuni.2021.06.012.
3. Chakravarthy A, Khan L, Bensler NP, Bose P, De Carvalho DD. TGF-β-associated extracellular matrix genes link cancer-associated fibroblasts to immune evasion and immunotherapy failure. Nature communications 2018;9(1):4692 doi 10.1038/s41467-018-06654-8.
4. Peng DH, Rodriguez BL, Diao L, Chen L, Wang J, Byers LA, et al. Collagen promotes anti-PD-1/PD-L1 resistance in cancer through LAIR1-dependent CD8(+) T cell exhaustion. Nature communications 2020;11(1):4520 doi 10.1038/s41467-020-18298-8.
5. Conklin MW, Eickhoff JC, Riching KM, Pehlke CA, Eliceiri KW, Provenzano PP, et al. Aligned collagen is a prognostic signature for survival in human breast carcinoma. The American journal of pathology 2011;178(3):1221–32 doi 10.1016/j.ajpath.2010.11.076.
6. Zhou ZH, Ji CD, Xiao HL, Zhao HB, Cui YH, Bian XW. Reorganized Collagen in the Tumor Microenvironment of Gastric Cancer and Its Association with Prognosis. Journal of Cancer 2017;8(8):1466–76 doi 10.7150/jca.18466.
7. Misawa K, Kanazawa T, Imai A, Endo S, Mochizuki D, Fukushima H, et al. Prognostic value of type XXII and XXIV collagen mRNA expression in head and neck cancer patients. Molecular and clinical oncology 2014;2(2):285–91 doi 10.3892/mco.2013.233.
8. Eble JA, Niland S. The extracellular matrix in tumor progression and metastasis. Clinical & experimental metastasis 2019;36(3):171–98 doi 10.1007/s10585-019-09966-1.
9. Kuczek DE, Larsen AMH, Thorseth ML, Carretta M, Kalvisa A, Siersbæk MS, et al. Collagen density regulates the activity of tumor-infiltrating T cells. Journal for immunotherapy of cancer 2019;7(1):68 doi 10.1186/s40425-019-0556-6.
10. Larsen AMH, Kuczek DE, Kalvisa A, Siersbæk MS, Thorseth ML, Johansen AZ, et al. Collagen Density Modulates the Immunosuppressive Functions of Macrophages. Journal of immunology (Baltimore, Md : 1950) 2020;205(5):1461–72 doi 10.4049/jimmunol.1900789.
11. O'Connor RS, Hao X, Shen K, Bashour K, Akimova T, Hancock WW, et al. Substrate rigidity regulates human T cell activation and proliferation. Journal of immunology (Baltimore, Md : 1950) 2012;189(3):1330–9 doi 10.4049/jimmunol.1102757.
12. Rygiel TP, Stolte EH, de Ruiter T, van de Weijer ML, Meyaard L. Tumor-expressed collagens can modulate immune cell function through the inhibitory collagen receptor LAIR-1. Molecular immunology 2011;49(1–2):402–6 doi 10.1016/j.molimm.2011.09.006.
13. Xu L, Wang S, Li J, Li J, Li B. Cancer immunotherapy based on blocking immune suppression mediated by an immune modulator LAIR-1. Oncoimmunology 2020;9(1):1740477 doi 10.1080/2162402x.2020.1740477.
14. Meyaard L, Hurenkamp J, Clevers H, Lanier LL, Phillips JH. Leukocyte-associated Ig-like receptor-1 functions as an inhibitory receptor on cytotoxic T cells. Journal of immunology (Baltimore, Md : 1950) 1999;162(10):5800–4.
15. Maasho K, Masilamani M, Valas R, Basu S, Coligan JE, Borrego F. The inhibitory leukocyte-associated Ig-like receptor-1 (LAIR-1) is expressed at high levels by human naive T cells and inhibits TCR mediated activation. Molecular immunology 2005;42(12):1521–30 doi 10.1016/j.molimm.2005.01.004.
16. Jansen CA, Cruijsen CW, de Ruiter T, Nanlohy N, Willems N, Janssens-Korpela PL, Meyaard L. Regulated expression of the inhibitory receptor LAIR-1 on human peripheral T cells during T cell activation and differentiation. European journal of immunology 2007;37(4):914–24 doi 10.1002/eji.200636678.
17. Lebbink RJ, van den Berg MC, de Ruiter T, Raynal N, van Roon JA, Lenting PJ, et al. The soluble leukocyte-associated Ig-like receptor (LAIR)-2 antagonizes the collagen/LAIR-1

inhibitory immune interaction. Journal of immunology (Baltimore, Md : 1950) 2008;180(3):1662–9 doi 10.4049/jimmunol.180.3.1662.

18. Horn LA, Chariou PL, Gameiro SR, Qin H, Iida M, et al. Remodeling the tumor microenvironment via blockade of LAIR-1 and TGF-β signaling enables PD-L1-mediated tumor eradication. Journal of Clinical Investigation 2022; 132(8): e155148 doi 10.1172/JCI155148.
19. Xie J, Gui X, Deng M, Chen H, Chen Y, Liu X, et al. Blocking LAIR1 signaling in immune cells inhibits tumor development. Frontiers in immunology 2022;13:996026 doi 10.3389/fimmu.2022.996026.
20. Verrecchia F, Chu ML, Mauviel A. Identification of novel TGF-beta /Smad gene targets in dermal fibroblasts using a combined cDNA microarray/promoter transactivation approach. The Journal of biological chemistry 2001;276(20):17058–62 doi 10.1074/jbc.M100754200.
21. Lambrechts D, Wauters E, Boeckx B, Aibar S, Nittner D, Burton O, et al. Phenotype molding of stromal cells in the lung tumor microenvironment. Nature medicine 2018;24(8):1277–89 doi 10.1038/s41591-018-0096-5.
22. Azizi E, Carr AJ, Plitas G, Cornish AE, Konopacki C, Prabhakaran S, et al. Single-Cell Map of Diverse Immune Phenotypes in the Breast Tumor Microenvironment. Cell 2018;174(5):1293–308.e36 doi 10.1016/j.cell.2018.05.060.
23. Peng J, Sun BF, Chen CY, Zhou JY, Chen YS, Chen H, et al. Single-cell RNA-seq highlights intra-tumoral heterogeneity and malignant progression in pancreatic ductal adenocarcinoma. Cell research 2019;29(9):725–38 doi 10.1038/s41422-019-0195-y.
24. Chen K, Wang Q, Li M, Guo H, Liu W, Wang F, et al. Single-cell RNA-seq reveals dynamic change in tumor microenvironment during pancreatic ductal adenocarcinoma malignant progression. EBioMedicine 2021;66:103315 doi 10.1016/j.ebiom.2021.103315.
25. Pelka K, Hofree M, Chen JH, Sarkizova S, Pirl JD, Jorgji V, et al. Spatially organized multicellular immune hubs in human colorectal cancer. Cell 2021;184(18):4734–52.e20 doi 10.1016/j.cell.2021.08.003.
26. Bi K, He MX, Bakouny Z, Kanodia A, Napolitano S, Wu J, et al. Tumor and immune reprogramming during immunotherapy in advanced renal cell carcinoma. Cancer cell 2021;39(5):649–61.e5 doi 10.1016/j.ccell.2021.02.015.
27. Kumar MP, Du J, Lagoudas G, Jiao Y, Sawyer A, Drummond DC, et al. Analysis of Single-Cell RNA-Seq Identifies Cell-Cell Communication Associated with Tumor Characteristics. Cell reports 2018;25(6):1458–68.e4 doi 10.1016/j.celrep.2018.10.047.
28. Gubin MM, Esaulova E, Ward JP, Malkova ON, Runci D, Wong P, et al. High-Dimensional Analysis Delineates Myeloid and Lymphoid Compartment Remodeling during Successful Immune-Checkpoint Cancer Therapy. Cell 2018;175(4):1014–30.e19 doi 10.1016/j.cell.2018.09.030.
29. Sade-Feldman M, Yizhak K, Bjorgaard SL, Ray JP, de Boer CG, Jenkins RW, et al. Defining T Cell States Associated with Response to Checkpoint Immunotherapy in Melanoma. Cell 2018;175(4):998–1013.e20 doi 10.1016/j.cell.2018.10.038.
30. McCarthy DJ, Chen Y, Smyth GK. Differential expression analysis of multifactor RNA-Seq experiments with respect to biological variation. Nucleic acids research 2012;40(10):4288–97 doi 10.1093/nar/gks042.
31. Robinson MD, McCarthy DJ, Smyth GK. edgeR: a Bioconductor package for differential expression analysis of digital gene expression data. Bioinformatics (Oxford, England) 2010;26(1):139–40 doi 10.1093/bioinformatics/btp616.
32. Goedhart J, Luijsterburg MS. VolcaNoseR is a web app for creating, exploring, labeling and sharing volcano plots. Scientific reports 2020;10(1):20560 doi 10.1038/s41598-020-76603-3.
33. Gibbons DL, Lin W, Creighton CJ, Rizvi ZH, Gregory PA, Goodall GJ, et al. Contextual extracellular cues promote tumor cell EMT and metastasis by regulating miR-200 family expression. Genes & development 2009;23(18):2140–51 doi 10.1101/gad.1820209.
34. Chen L, Gibbons DL, Goswami S, Cortez MA, Ahn YH, Byers LA, et al. Metastasis is regulated via microRNA-200/ZEB1 axis control of tumour cell PD-L1 expression and intratumoral immunosuppression. Nature communications 2014;5:5241 doi 10.1038/ncomms6241.

35. Zheng S, El-Naggar AK, Kim ES, Kurie JM, Lozano G. A genetic mouse model for metastatic lung cancer with gender differences in survival. Oncogene 2007;26(48):6896–904 doi 10.1038/sj.onc.1210493.
36. Dobin A, Davis CA, Schlesinger F, Drenkow J, Zaleski C, Jha S, et al. STAR: ultrafast universal RNA-seq aligner. Bioinformatics (Oxford, England) 2013;29(1):15–21 doi 10.1093/bioinformatics/bts635.
37. Liao Y, Smyth GK, Shi W. featureCounts: an efficient general purpose program for assigning sequence reads to genomic features. Bioinformatics (Oxford, England) 2014;30(7):923–30 doi 10.1093/bioinformatics/btt656.
38. Chen DS, Mellman I. Elements of cancer immunity and the cancer-immune set point. Nature 2017;541(7637):321–30 doi 10.1038/nature21349.
39. Krämer A, Green J, Pollard J Jr., Tugendreich S. Causal analysis approaches in Ingenuity Pathway Analysis. Bioinformatics (Oxford, England) 2014;30(4):523–30 doi 10.1093/bioinformatics/btt703.
40. Wei P, Zhao YG, Zhuang L, Ruben S, Sang QX. Expression and enzymatic activity of human disintegrin and metalloproteinase ADAM19/meltrin beta. Biochemical and biophysical research communications 2001;280(3):744–55 doi 10.1006/bbrc.2000.4200.
41. Ding J, Meng Y, Han Z, Luo X, Guo X, Li Y, et al. Pan-Cancer Analysis of the Oncogenic and Immunological Role of RCN3: A Potential Biomarker for Prognosis and Immunotherapy. Frontiers in oncology 2022;12:811567 doi 10.3389/fonc.2022.811567.
42. Tsuboi S. Requirement for a complex of Wiskott-Aldrich syndrome protein (WASP) with WASP interacting protein in podosome formation in macrophages. Journal of immunology (Baltimore, Md : 1950) 2007;178(5):2987–95 doi 10.4049/jimmunol.178.5.2987.
43. Franke WW, Goldschmidt MD, Zimbelmann R, Mueller HM, Schiller DL, Cowin P. Molecular cloning and amino acid sequence of human plakoglobin, the common junctional plaque protein. Proceedings of the National Academy of Sciences of the United States of America 1989;86(11):4027–31 doi 10.1073/pnas.86.11.4027.
44. Kotaka M, Kostin S, Ngai S, Chan K, Lau Y, Lee SM, et al. Interaction of hCLIM1, an enigma family protein, with alpha-actinin 2. Journal of cellular biochemistry 2000;78(4):558–65 doi 10.1002/1097-4644(20000915)78:4<558::aid-jcb5>3.0.co;2-i.
45. Crawley SC, Fan B, Li BC, Rivera LB, Sissons JR, Sitrin J, et al., inventors; NGM Biopharmaceuticals, Inc., assignee. LAIR-1-binding agents and methods of use thereof. United States patent application publication US 2022/0041711 A1. 2022 Feb 10.
46. Chen L, Diao L, Yang Y, Yi X, Rodriguez BL, Li Y, et al. CD38-Mediated Immunosuppression as a Mechanism of Tumor Cell Escape from PD-1/PD-L1 Blockade. Cancer Discov 2018;8(9):1156–75 doi 10.1158/2159-8290.CD-17-1033.
47. Rodriguez BL, Chen L, Li Y, Miao S, Peng DH, Fradette JJ, et al. Targeting immunosuppressive Ly6C+ classical monocytes reverses anti-PD-1/CTLA-4 immunotherapy resistance. Frontiers in immunology 2023;14:1161869 doi 10.3389/fimmu.2023.1161869.
48. Peng DH, Kundu ST, Fradette JJ, Diao L, Tong P, Byers LA, et al. ZEB1 suppression sensitizes KRAS mutant cancers to MEK inhibition by an IL17RD-dependent mechanism. Science translational medicine 2019;11(483) doi 10.1126/scitranslmed.aaq1238.
49. Lebbink RJ, de Ruiter T, Adelmeijer J, Brenkman AB, van Helvoort JM, Koch M, et al. Collagens are functional, high affinity ligands for the inhibitory immune receptor LAIR-1. The Journal of experimental medicine 2006;203(6):1419–25 doi 10.1084/jem.20052554.
50. Rømer AMA, Thorseth ML, Madsen DH. Immune Modulatory Properties of Collagen in Cancer. Frontiers in immunology 2021;12:791453 doi 10.3389/fimmu.2021.791453.
51. Valkenburg KC, de Groot AE, Pienta KJ. Targeting the tumour stroma to improve cancer therapy. Nature reviews Clinical oncology 2018;15(6):366–81 doi 10.1038/s41571-018-0007-1.
52. Kraman M, Bambrough PJ, Arnold JN, Roberts EW, Magiera L, Jones JO, et al. Suppression of antitumor immunity by stromal cells expressing fibroblast activation protein-alpha. Science (New York, NY) 2010;330(6005):827–30 doi 10.1126/science.1195300.
53. Cassetta L, Pollard JW. A timeline of tumour-associated macrophage biology. Nature reviews Cancer 2023;23(4):238–57 doi 10.1038/s41568-022-00547-1.

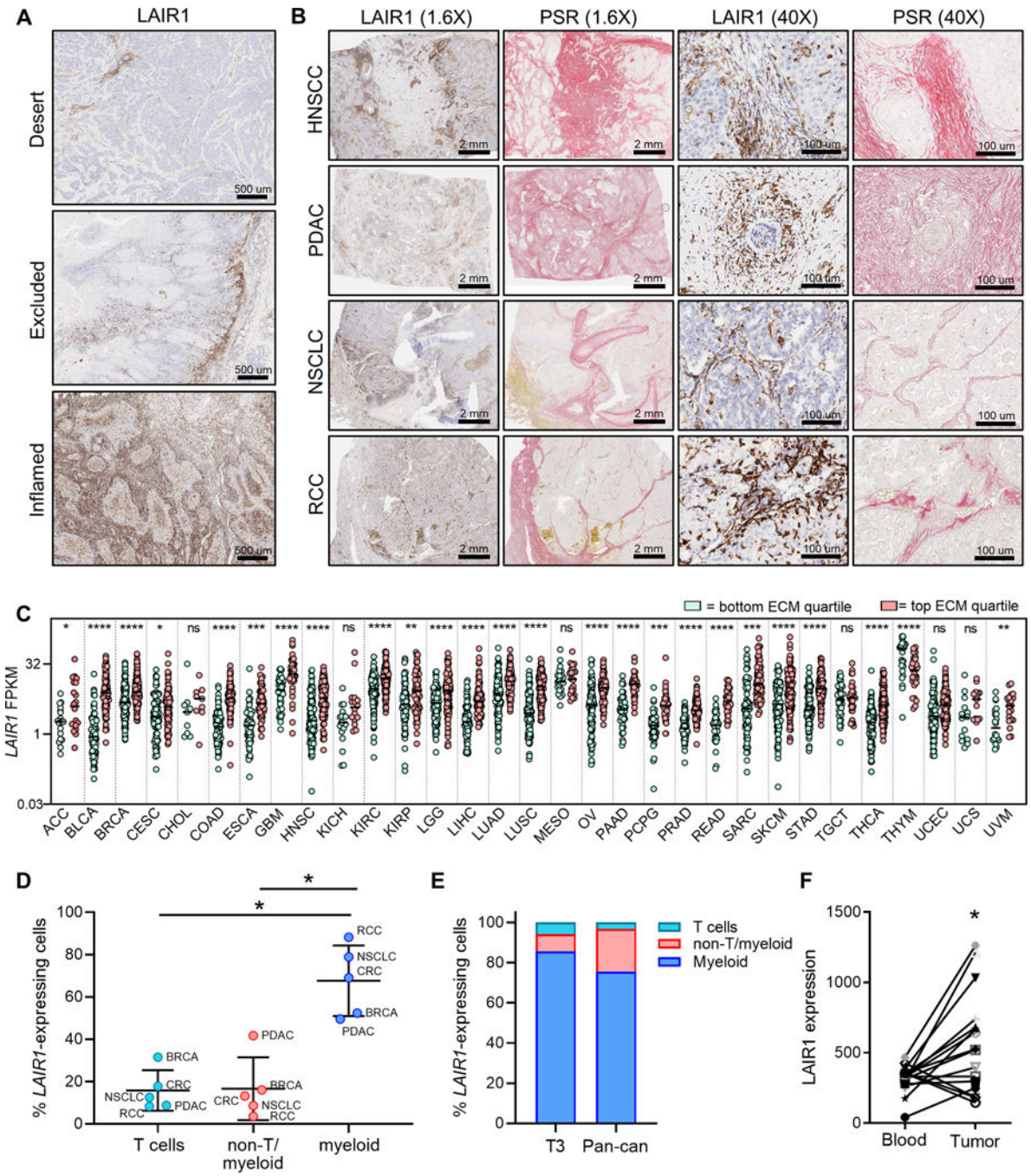

Figure 1.

LAIR1 expression in solid cancers is associated with stroma and myeloid cells. **A,** IHC detection of LAIR1 in human HNSCC tumors exhibiting the indicated immune phenotypes. **B,** Co-distribution of LAIR1 and stroma in human tumors. LAIR1 and stroma were detected in proximal RCC, NSCLC, PDAC, HNSCC sections via IHC and PSR respectively. **C,** LAIR1 expression in ECM-high versus ECM-low tumors (TCGA). LAIR1 FPKM is plotted for tumors scoring in either the top or bottom quartiles for ECM gene expression. Statistical significance was assessed using an unpaired, two-tailed T test. **D,** Patient matched LAIR1

expression on intratumoral and circulating CD45+CD15-CD14+CD11b+ myeloid cells (n = 16 patients). Statistical significance was assessed using a paired, two-tailed T test (move to end of figure). **E and F,** Composition of LAIR1-expressing cells in human and murine tumors. Lineage-separated LAIR1-expressing cell abundance was assessed in scRNAseq datasets derived from primary human (E) and syngeneic mouse (F) tumors. Statistical significance was assessed using a paired, two-tailed T test. *, $p < 0.05$; **, $p < 0.005$; ***, $p < 0.0005$; ****, $p < 0.00005$; ns, not significant.

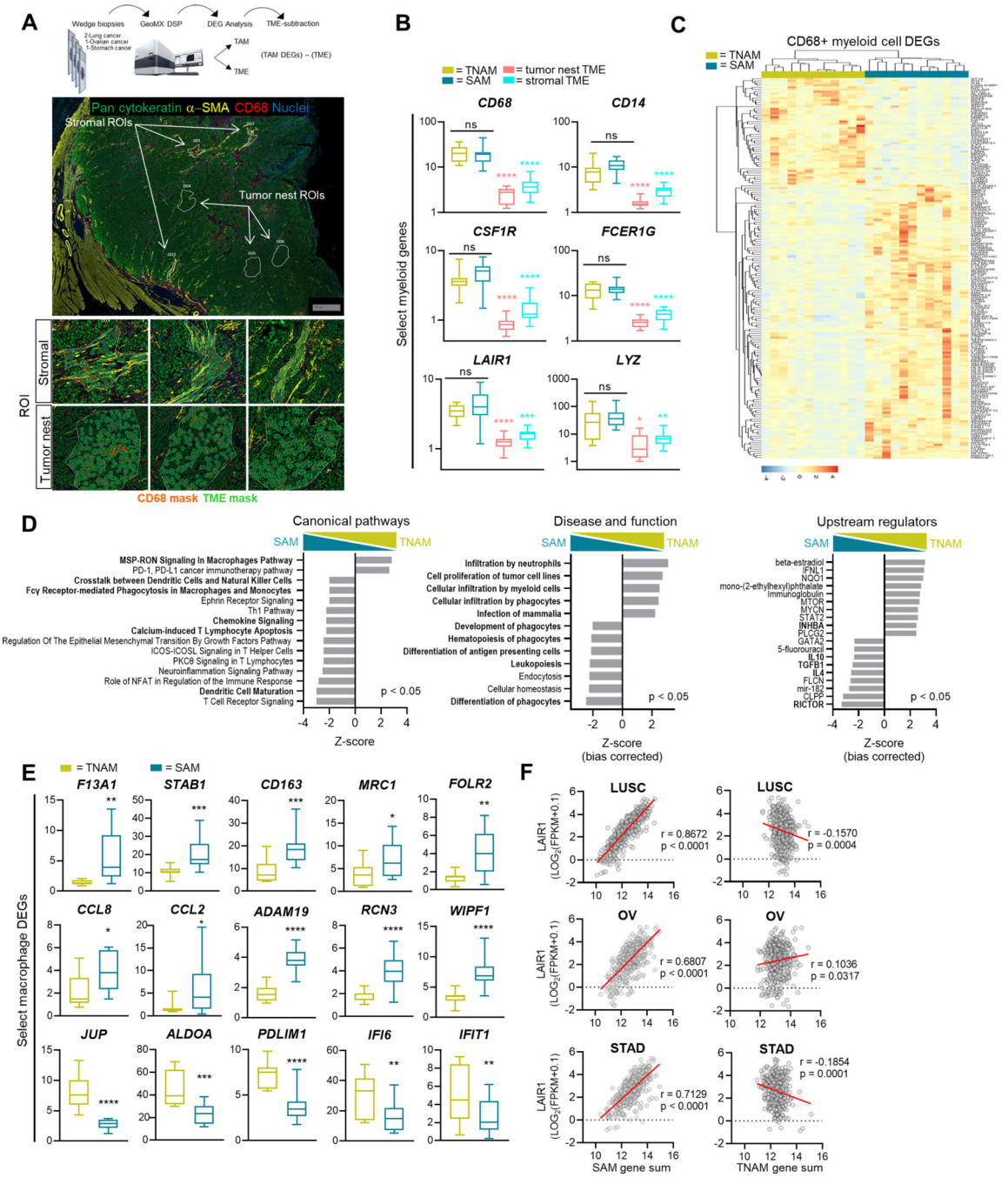

Figure 2.

Stroma elicits a distinct and suppressive phenotype in tumor-associated myeloid cells.

A, Selection of stroma- and tumor nest-associated myeloid cells in human tumors for digital spatial transcriptomic profiling. Top: schematic of workflow for ROI selection. Four human tumor FFPE sections were first subjected to a whole transcriptome GeoMx assay (Nanostring); DEG analysis was then performed to identify genes expressed in myeloid cells and their adjacent TMEs. Bottom: staining strategy used to identify ROIs. Anti-α-SMA was used to visualize stroma, anti-Pan-cytokeratin to visualize tumor cells, and anti-CD68

to visualize myeloid cells. Stromal and tumor nest ROIs were selected first, and within these, CD68 (SAM and TNAM) and TME (stroma and tumor nest) masks were applied for subsequent transcriptomic analysis. FFPE tumors used for this analysis included one ovarian, one gastric, and two squamous lung cancers. Three stromal and three tumor nest ROIs were selected per FFPE section. **B,** *LAIR1* and myeloid gene expression in CD68+ cells within stroma and tumor nests. Box and whisker plots with min to max of Q3-normalized counts are shown for the indicated TME and CD68 masks (n = 12 per mask). Statistical significance was assessed using an unpaired, two-tailed T test. TME p values are versus their constituent myeloid populations. **C,** Genes differentially expressed between SAM and TNAM. DEG analysis was performed using cut offs of p value < 0.05 and fold change > 2, followed by removal of TME genes. N = 12 per mask. **D,** IPA analysis of TME-subtracted SAM and TNAM DEGs. Canonical pathway, disease and biology functions, and upstream regulator analyses were performed, and top pathways were identified using a Z score > 2 and p value < 0.05. Pathways favoring SAM point left, and those favoring TNAM point right. **E,** Expression of select genes in SAM and TNAM after TME subtraction. Box and whisker plots with min to max Q3-normalized counts are shown for the indicated TME-subtracted CD68 masks (n = 12 per mask). Statistical significance was assessed using an unpaired, two-tailed T test. **F,** Correlation of LAIR1 prevalence with compartmentalized intratumoral myeloid cells (TCGA). Pearson correlation (red line) for *LAIR1* with genes overexpressed in SAM or TNAM was assessed in OV, STAD, and LUSC. *, p < 0.05; **, p < 0.005; ***, p < 0.0005; ****, p < 0.00005; ns, not significant.

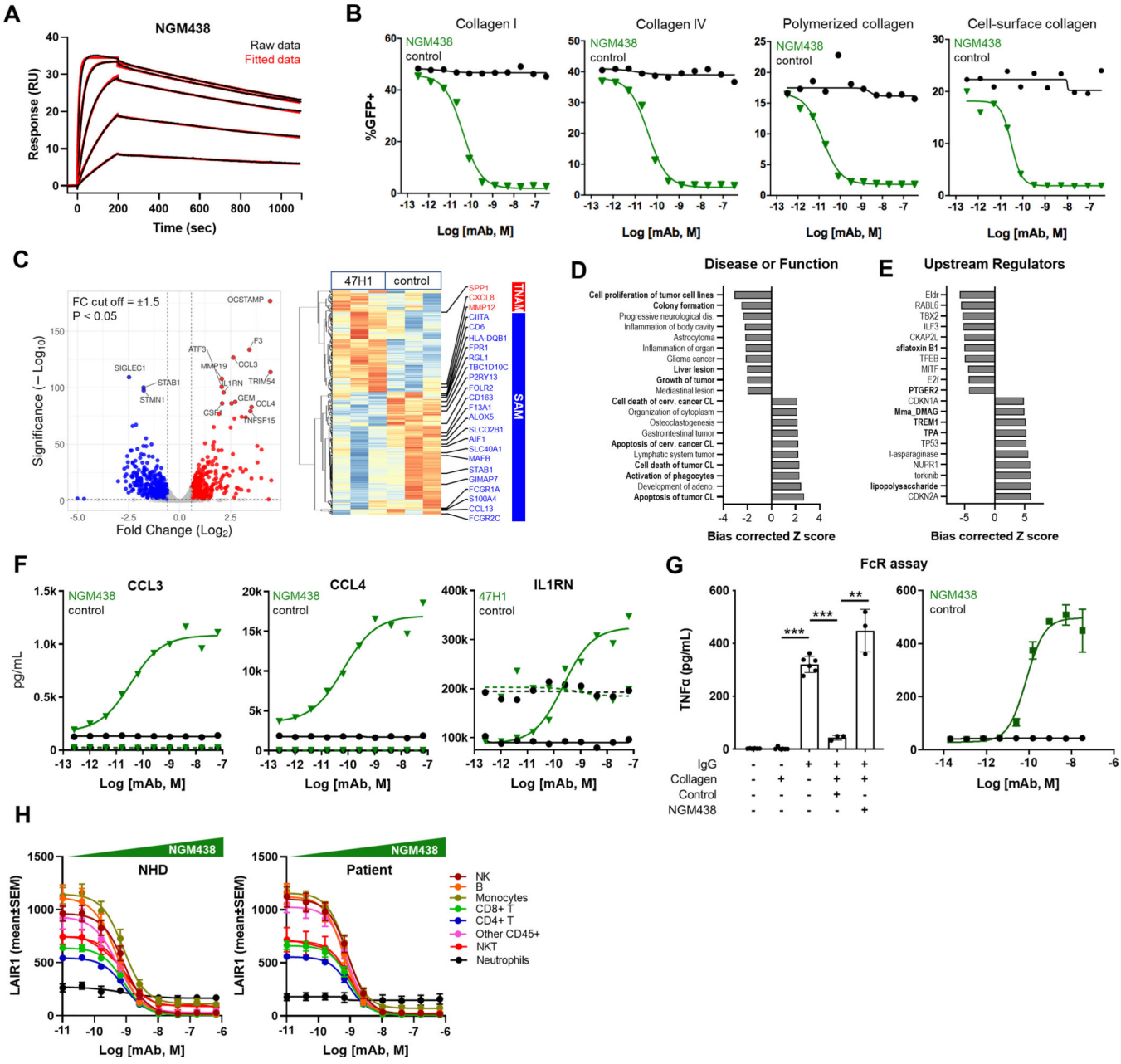

Figure 3.

NGM438 binds LAIR1 and blocks LAIR1/collagen engagement. **A,** NGM438 directly binds LAIR1 as detected by surface plasmon resonance. Representative data from a single experiment is shown. Binding studies were performed at least three times. **B,** NGM438 blocks LAIR1 from binding to collagen. LAIR1-GFP reporter cells were mixed with NGM438 or an anti-KLH control antibody and incubated on reconstituted collagen extracts, basement membrane, or collagen-expressing bEnd.3 cells as indicated. Percent of collagen-induced GFP expressing cells are plotted. Data are representative from at least three independent experiments. **C,** DEG analysis of human monocyte-derived dendritic cells treated with the NGM438 parental clone 47H1 or anti-KLH control using the indicated

cutoffs. FC, fold change. Data are pooled from three distinct donors. DEGs identified are plotted in the heatmap on the right. Statistical significance was assessed using a paired, two-tailed T test. **D** and **E,** IPA analysis of DEGs regulated by LAIR1. Disease and biology functions (D), and upstream regulator (E) analyses were performed on DEGs identified in C, and top pathways were identified using a Z score > 2 and p value < 0.05. **F**, NGM438-induced, collagen driven myeloid inflammation. Monocyte-derived dendritic cells were mixed with NGM438 or 47H1 and incubated either on collagen I-coated (solid lines) or uncoated (dashed lines) surfaces. Secreted CCL3, CCL4, and IL1RN were measured in conditioned media. Data are representative from at least three independent experiments and donors. **G,** NGM438-induced, FcR-driven TNFα secretion. Monocyte-derived dendritic cells were mixed with NGM438 or anti-KLH control at increasing concentrations and subjected to IgG-driven Fc-receptor stimulation in the presence of collagen as indicated. Secreted TNFα was measured in conditioned media. Data are representative from at least three independent experiments and donors. Mean ± SD is shown. Dose dependent induction of TNFα is shown on the right. Statistical significance was assessed using an unpaired, two-tailed T test. **H,** NGM438 binds LAIR1 on circulating immune cell populations. Whole blood from NHD or cancer patients was incubated with NGM438 then subjected to a LAIR1 occupancy assay. MFI of LAIR1 unoccupied by NGM438 is shown and was assessed using FACS. NHD n = 9; patient n = 10. **, $p < 0.005$; ***, $p < 0.0005$.

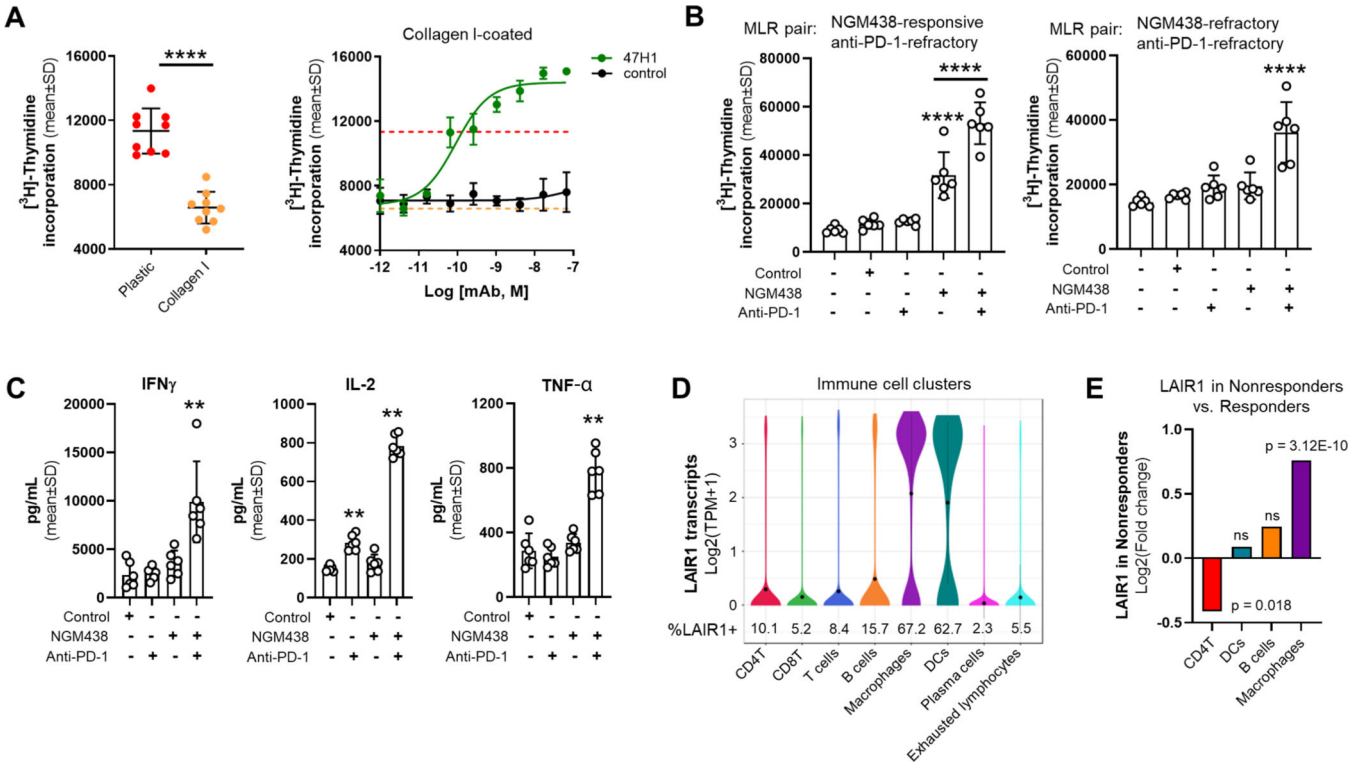

Figure 4.

LAIR1 is associated with resistance to anti-PD-1. **A,** LAIR1 mediates collagen suppression of T cell proliferation in a mixed lymphocyte reaction. Pan-T cells were mixed with allogeneic monocyte-derived dendritic cells and incubated either on plastic or collagen I-coated surfaces. T cell proliferation was assessed using [H^3]-thymidine incorporation. Data shown are from a single donor pair and are representative of at least three independent experiments and donor pairs. Data to the right show dose dependent rescue of collagen driven suppression by clone 47H1. Orange dashed line = mean incorporation on plastic; yellow dashed line = mean incorporation on collagen. **B,** Combined NGM438 and anti-PD-1 enhance T-cell proliferation in collagen-treated mixed lymphocytes reactions. [H^3]-thymidine incorporation is shown from two donor pairs and is representative of three independent experiments and donor pairs. **C,** Combined NGM438 and anti-PD-1 enhance cytokine secretion in collagen-treated mixed lymphocytes reactions. Cytokines were measured in conditioned media one day prior to assessing proliferation. Statistical significance in C and D was assessed using an unpaired two-tailed T test and is noted versus control unless otherwise indicated. **D,** Baseline *LAIR1* expression in melanoma tumors from 19 patients that went on to receive checkpoint therapy. Left: violin plots of LAIR1 transcripts across immune cell subsets identified using scRNAseq (GSE120575). % of cells expressing *LAIR1* is indicated. **E,** Fold change LAIR1 expression in patients that went on to respond to checkpoint therapy versus nonresponders. Statistical significance was assessed using Seurat. Responders, n = 10; nonresponders n = 9. **, $p < 0.005$; ****, $p < 0.00005$.

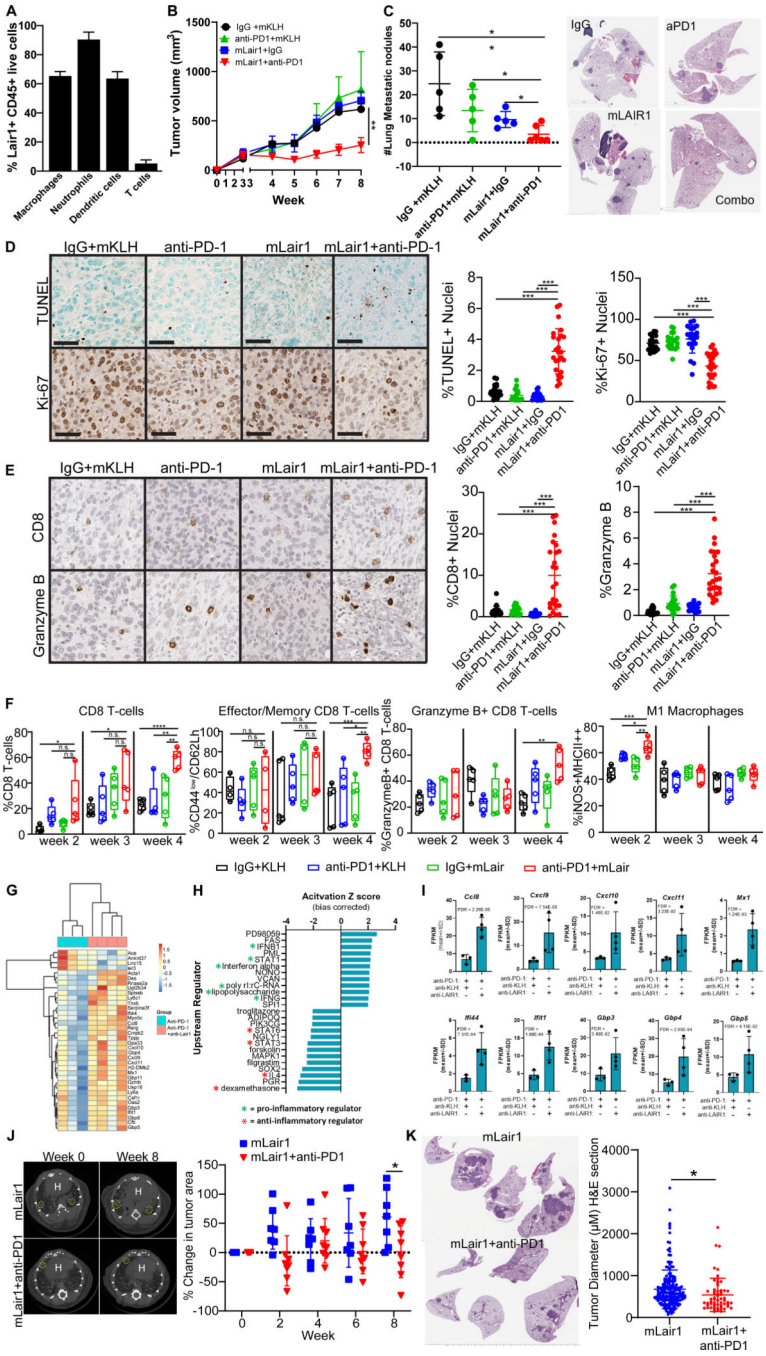

Figure 5.

LAIR1-blockade sensitizes stroma-dense, anti-PD-1 refractory mouse tumors to therapy. **A**, Percentage LAIR1+ in 344SQ tumor, macrophages (CD11b+, CD11C-, F4/80+), neutrophils (Ly6G+ Ly6C-), dendritic cells (CD11b-F4/80-CD11C+), and T cells (CD3+CD19-CD45+). **B**, *in vivo* tumor volume at indicated time points for 344SQ subcutaneous tumors in syngeneic wild-type mice. Treatment groups include anti-LAIR1, anti-PD-1, or combination of anti-LAIR1/PD-1 or isotype control. **C**, Quantitation of lung metastatic surface nodules from indicated experimental groups from (B) at the endpoint of treatments. **D**,

Representative images of TUNEL (top) and Ki-67 (bottom) IHC staining in primary tumors formed by 344SQ tumors after 8 weeks of treatment. Quantitation found on right. **E**, Representative images of CD8 (top) and Granzyme-B (bottom) IHC staining in primary tumors formed by 344SQ tumors after 8 weeks of treatment. Quantitation found on right. **F**, Percentage of total CD8 CD3 CD45 T cells in tumors harvested at week 2, week 3, and week 4. Percentage of $CD44^{low}$ CD62L+ CD8 CD3 T cells effector/memory CD8 T cells. Percentage of granzyme-B CD8 CD3 T cells. Percentage of iNOS+MHCII++ M1 macrophages. **G**, Heatmap of genes from RNAseq analysis of 344SQ tumors treated with anti-PD-1 (blue) and anti-LAIR1/PD-1 combination (pink) at week 4 using a fold change cut off of 1.5 with FDR < 0.05. **H,** IPA analysis of upstream regulators using DEGs identified in **G**. Top pathways are shown after using cut offs of Z score > 2, $p < 0.05$. **I,** Select interferon-inducible genes identified in **G. J**, Representative micro-CT images of $Kras^{LSL\text{-}G12D}/p53^{fl/fl}$ lungs at week 0 and week 8. Yellow dashed circles outline target lesions. “H” indicates the mouse heart. The percentage of tumor area change during treatment during week 2, 4, 6, and 8. **K**, Representative H&E of mouse lungs from L at week 8 (left). Quantification of tumor diameter on H&E-stained lungs from $Kras^{LSL\text{-}G12D}/p53^{fl/fl}$ mice treated with mLAIR1 or mLAIR1/PD-1 (right). Data were analyzed using unpaired Students *t* test. *P<0.05; **P<0.01; ***P<0.001; ****P<0.0001; n.s. not significant.